PHILIPPINE ENGINEERING JOURNAL
PEJ 2023; Vol. 44, No. 2: 1-24

Received: 03 June 2023
Accepted: 11 November 2023

Development of the Damage Attribution Chart Identifying the Wind-Susceptible Building Component by Incorporating Fault-Tree Analysis into the Component-based Vulnerability Modelling Against Severe Wind – A Case of the Philippine Public-School Building

Liezl Raissa E. Tan and Jaime Y. Hernandez Jr.
Institute of Civil Engineering
University of the Philippines Diliman, 1101 Quezon City, Philippines
Corresponding author: letan@up.edu.ph

Abstract *– The component-based approach in vulnerability modelling can estimate the amount of damage per vulnerable building component. However, it cannot identify the source of failure. Hence, this study incorporates a fault-tree analysis into the vulnerability model in order to identify the susceptible component. Thereby developing a systematic framework that aids in directing where building strengthening efforts must be applied. The framework is applied to a one-story, three-bay public-school building, where the vulnerable building components identified and being monitored includes the roof fastener, roof cover, purlin connection, purlin section, roof-to-column connection, and the window panels. The building is subjected to wind pressures estimated using the computational fluid dynamics (CFD) modelled in ANSYS and calibrated with a wind tunnel test. These loadings together with the probabilistic resistance capacities determined for the identified vulnerable components are fed into the Monte-Carlo simulation with fault-tree algorithm to quantify and classify the damage. The failure simulation produces what this study coined as the damage attribution chart that shows which building component can the damages be attributed to. The resulting critical component for the case study considered is the roof-to-column connection. This was validated against a field survey conducted to a similar school building that was damaged by the Typhoon Odette, which shows similar damages as simulated. The study further investigates the effects of strengthening various building components which suggests that not all strengthening mitigations would lead to the reduction of the overall building damage.*

Keywords*: Damage Attribution Chart; Component-based Reliability Modelling; Wind Vulnerability Curves; Design Optimization and Retrofit.*

I. INTRODUCTION

Strengthening of roof covers and fasteners, which are seen prominently damaged during typhoon events, are common mitigations applied post-disaster. It supposes that strengthening the vulnerable building components that are commonly seen post-disaster will reduce the damage incurred by the building due to severe wind. However, strengthening one component must consider the effect on the entire structure, since increasing the capacity of a building component will redistribute the forces into other building components which could lead to greater damage to the structure. A similar conclusion was obtained in a collaborative project between the Department of Science and Technology (DOST) and Japan Science and

Technology (JST) [10] as they investigated the wind damage processes to a non-engineered house in Leyte due to Typhoon Yolanda. The said project identified three weak points where failure is being monitored. These include the roof cover, roof-to-column connection, and column-to-foundation connection. They found that as the resistance of the roof cover increases, the roof panels tend to carry higher wind loads and consequently transfer these loads toward the connections increasing the failure probability of the connections. Although this observation simply follows the concept of load path, the study further highlighted the implication of strengthening portions of the building to the overall detriment of the structure. Failure of connections, for example, may greatly affect the stability of the structure which may lead to collapse while the failure of the roof panel is localized and does not necessarily affect the structural integrity, hence greater damage might result from the former. The study concluded with a lesson, that not all strengthening mitigations would lead to lesser damage. Rather, these mitigations must be further evaluated considering the response of the entire structure. If so, then the results of this study pose the problem on how can the critical building component be identified and how can the improvement be measured.

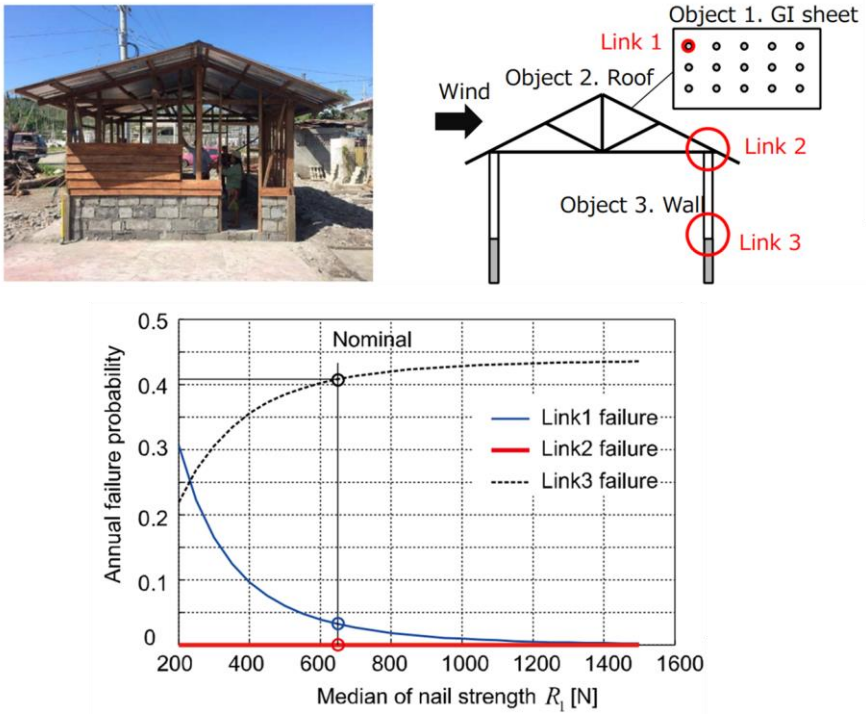

Figure 1. (a) Sample photo and (b) sketch of a typical non-engineered house in Leyte labelled with the identified weak links. (c) Failure probability vs. resistance of the identified weak links. (Nishijima, et al. 2015)

Following through this idea, this paper aims to develop a framework in determining the critical building component that leads to greatest overall structural damage. Whereby strengthening of the identified critical component will result to the greatest reduction of damage. The output of this study can be used in optimizing building design or retrofitting recommendations against the severe wind.

1.1 Vulnerability Curves

To recommend a particular building design, its corresponding performance must be evaluated. One of the models that can be utilized to assess the building's performance is the vulnerability curve. A vulnerability curve is a plot of the measure of the damage incurred by a building for a particular hazard intensity [19]. The local wind speed is used as a measure of the hazard intensity, while the ratio of the repair cost to the construction cost or the damage ratio is used as a measure of the damage.

Vulnerability curves have a wide application in disaster risk management. It is used in the prediction model of disaster risk that aids the local government units in planning, response, and mitigation efforts. Vulnerability curves can also be used as a reference in setting building insurance premiums.

This study is particularly interested in the use of vulnerability curves in evaluating the relative performances of various building design cases. This approach was implemented in the papers of Torkian et al.[16] when they evaluated the cost-benefit of various windstorm mitigation measures for buildings in Florida. Although the vulnerability curves can determine which design schemes provide a better building performance, it does not identify which building component is susceptible to damage. To determine the optimal strengthening scheme, the vulnerability curve can only provide an assessment but cannot provide a structured selection on which strengthening scheme must be employed. And this is what the study is trying to address.

1.2 Component-based Reliability Approach

There are many ways in developing the vulnerability curve. One method of particular interest is the component-based approach as it enables the quantification of damage per building components. In this way, the propagation of damage can be tracked making this approach suitable for identifying the critical building components that cause most of the damage.

Studies of Unanwa, et al. [18], Cope, A. [4], Pinelli [11], and Goyal, et al. [8] employ the component-based approach. These studies started with the identification of the vulnerable structure components where failure probability is estimated. This is followed by hazard modelling, wherein only Zhang, et al. [20] employ a probabilistic wind load while the rest assumed a deterministic wind load. In Cope's [4] study, the wind load was estimated using the design codes for both the external pressures and internal pressures, while Zhang's [20] study estimated the wind load from a wind tunnel test. Both Zhang [20] and Cope [4] considers the induced internal pressures due to the partial removal of the building envelope resulting from damages to the roof panel/cover and window panes. Cope [4] estimated the induced internal pressure as the weighted average of the pressure at the location of the broken doors and windows while Zhang [20] estimated the internal pressure as the average of the external pressures at the location of the damaged windows.

When it comes to the component resistance capacities, the aforementioned studies employ a probabilistic model following a lognormal distribution. In Cope's [4] study, the probabilistic resistance capacities were obtained from available literature and manufacturer data.

In terms of failure modelling, Unanwa [18] considers the interaction of the damage induced directly from the given hazard and the damage propagated from the damage of other components. Moreover, damage to various components caused by the hazard event was considered by imposing the common mode effect. To aid in the interdependence of component failure from each other, a fault tree analysis was also employed. The component location parameter, α_i, accounts for the location and distribution of building components to their degrees of wind damage. It considers the fact that failure of one item of a component does not necessarily imply total damage to the component. This parameter is obtained via expert experience using the Delphi method. Cope's [4] study considers the dependency of building components on each other, while Zhang's [20] failure model for each building component assumes they are independent of each other, and hence direct load-resistance comparison will define the failure of that component. Cope [4] did consider the failure dependency of each building component, however, wind loading on the components was roughly based on the tributary area method, especially for the roof-to-wall connection.

Pinelli [11] and Unanwa [18], mainly focus on the aggregation of damage to form a vulnerability model and hence start with hypothetical inputs including the wind load and the resistances used in the simulation. Unanwa [18] proposed a model that determines the wind damage band of any building or group of buildings. In this model, the failure probabilities per component were multiplied by the corresponding cost component factor (CCF) thus providing a way to aggregate the damage for the entire building.

Validation of the structural damage probability in Cope's [4] study was done using damage reports but only to a certain extent, and is limited by the quality of the damage data coming from the National Association of Home Builders Research Center (NAHB). While Pinelli [11] used insurance claim data to validate the exterior and interior building damage.

II. METHODOLOGY

This study utilizes the component-based reliability approach in vulnerability modelling. The building is first discretised by building components and then each component is discretised into elements – it could be an area element for panels and sheets, line element for members and frames, and point for connections and fasteners. Each element was assigned with its associated resistance capacities that were determined from either material testing, literature, or their nominal design strength. The failure of each element is assessed by comparing its resistance capacity with the corresponding load effects that were simulated from a structural analysis. The loading applied in the structural analysis is simulated by conducting a computational fluid dynamic (CFD) using ANSYS [2]. Failure is defined when the load effect exceeded the resistance, and the element is regarded as damaged. These damages are being monitored for every building element and are counted by building component, which is referred to in this study as the damage count. The damage count of a building component divided by its total number of discretised elements will provide the percent damage of that building component. But the same cannot be done in getting the percent damage of the entire building since the damage in one component may differ in impact in terms of performance and cost from another component. Hence, in order to aggregate the damage counts from various

building components, the study adapted the cost component factor (CCF) used by Pinelli [11] and Unanwa [18]. The cost component factor is quantified by taking the ratio of the cost of repairing the entire building component to the total cost of construction. Multiplying the CCF to the building component's percent damage converts it to the ratio of the cost of repair of damage to the total construction cost defined as the damage ratio. The damage ratios from various building components can now be aggregated since everything is valuated in terms of cost ratios. Hence, the damage ratio can now represent the measure of damage of the entire building in the vulnerability curve.

Although the vulnerability curves provide a relative evaluation of the building performances associated with a particular strengthening scheme, it cannot identify the source of failure where one would logically initiate any strengthening scheme. In order to identify the source of failure, the study added an extra step of putting tabs on the damage counts before proceeding to damage aggregation. Hence, the damage counts per building components were first classified into direct damages and then to propagated damages. The propagated damages were further associated with the failure of the underlying components to which the source of damage can be attributed. These stored values of the damage counts will then be used in creating the damage attribution chart.

2.1 Identification of the Vulnerable Building Components and their Corresponding Failure Modes

The study started with identifying the critical building components where failure is evaluated and their corresponding failure modes. As a demonstration, the concept will be applied to a one-story, three-bay public-school building. The critical components identified include the roof cover, roof-truss-to-column connections, purlin connections, purlin sections, and window panels, which are illustrated in Figure 2. These were determined based on commonly observed damages during the post-Typhoon Yolanda survey in Leyte. Other components, such as ceiling, door, tie rods, and sag rods among others, were not considered because they either are not frequently present in the structure, not commonly damaged, or has very little effect to structural performance and cost.

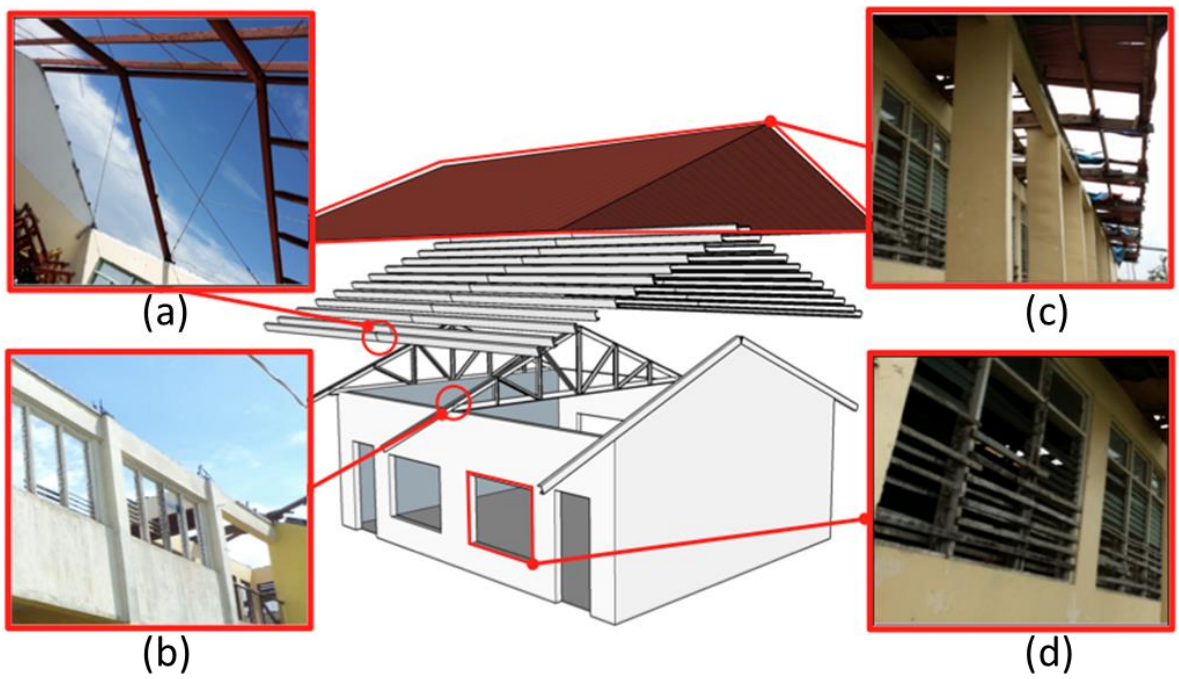

Figure 2.Commonly observed damages in buildings during the post-Yolanda survey. (a) Failure at the weld connection between purlins and roof truss/rafter, (b) unbending of the extended longitudinal rebars from the column that connects to the roof truss, (c) roof sheet failure either by nail pull-out or pull-thru, and (d) window jalousie breakage.

The failure modes associated with the roof cover include the failure of the connection between the roof fastener and the purlin through pull-out and the failure of the connection between the roof fastener and the roof cover due to the tearing of the roof sheets also known as pull-through [10].

For the roof-truss-to-column connections, which are typically made of extended longitudinal rebars wrapped around the truss, the corresponding failure mode observed in the field is the unbending of the rebars. While for the purlin connections, since it comprises angle bars welded to both the purlin and the roof truss, the corresponding failure mode is the failure of the weld connection. Purlin section failure was assumed to occur when the fiber yield stress of 248 MPa, based on the nominal capacity, was exceeded by the maximum fiber stress from the unsymmetric biaxial bending of the purlin section. Lastly, the failure of the window panel was defined when the local pressure on the window panel exceeds the estimated load resistance.

2.2 Resistance Capacities

Resistance capacities of the various identified failure modes were quantified which were based on either material tests, existing literature, or their nominal design strengths. These are summarized in Table 1.

Table 1. Summary of resistance capacities.

Building Elements	***Mean***	***COV***	***Distribution***	***Reference***
RCC (rebars)	12.28 kN	0.613	Lognormal	Material Test by Doguiles (2015) [5]
RCC (Anchor bolt)	8.82 MN	0.2	Lognormal	Literature Cope (2004)[4]
Purlin Section	248 MPa	0	Deterministic	Nominal Capacity
Purlin Connection	232.25 kN	0.063	Lognormal	Literature Kanvinde (2008)[9]
Roof Fastener: Tek Screw (Pull-Out)	538.7 N	0.1	Lognormal	Material Test by Bisa (2013) [3], Nishijima (2015) [10]
Roof Fastener: Tek Screw (Pull-Thru)	1467.8 N	0.09	Lognormal	
Roof Fastener: J-bolt (pull-out)	2829.1 N	0.08	Logistic	Material Test by Sanidad (2014) [12]
Roof Fastener: J-bolt (pull-thru)	1817.84 N	0.21	Lognormal	
Window Panel	2.5 kPa	0.2	Gaussian	Literature, ASTM E1300 [1]

2.3 Wind Load Modelling

To estimate the wind pressure around the building envelope, a computational fluid dynamic (CFD) model was implemented using ANSYS. The numerical model was validated and calibrated using the TPU aerodynamic database of isolated low-rise building with eaves that was conducted by Tokyo Polytechnic University (TPU) [17]. The closest geometry to the case study in this paper is that of roof type C with height to depth ratio of 1:4.

The pressure test was conducted in an open-circuit, low-speed type boundary layer wind tunnel. It has a test section of 1.2 wide, 1.0 m high and 14 m long. The wind speed ranges from 0.2 to 15 m/s. The velocity profile follows the Power Law equation having a roughness coefficient equal to 0.20. The length scale, velocity scale, and time scale used are 1:100, 1:3, and 3:100, respectively.

The CFD modelling employs full-scale dimensions. The enclosure dimensions used were patterned after the dimensions of the test section. A global fine mesh with curvature and proximity refinement was implemented with local sizing of 0.1 m maximum mesh size applied on all the building surfaces and local inflation layers of 15 was applied on all the building surfaces and the ground.

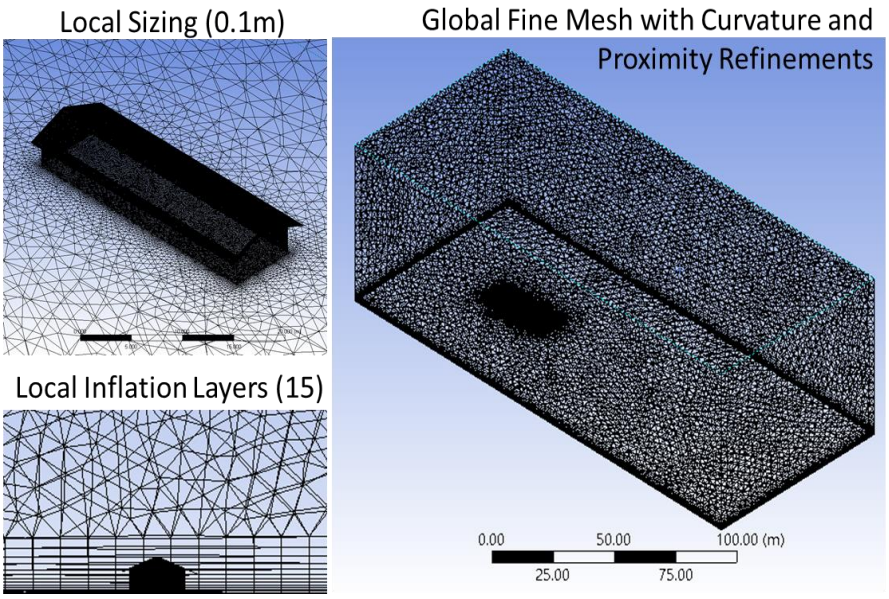

Figure 3. Mesh parameters used in the numerical modelling.

The velocity profile developed in the wind tunnel test was assigned at the inlet of the CFD simulation with a turbulence intensity of 10%. A zero-reference average static pressure with a 5% pressure blend was assigned at the outlet. The side walls and the top wall of the enclosure were assigned with free-slip wall boundary condition while the ground and the building surfaces were assigned with a no-slip wall.

The fluid used was isothermal air following the ideal gas at 25 0C. The turbulence model used was the Shear Stress Transport Model (SST) employing Reynold's Averaged Navier-Stokes (RANS) equations for the numerical method with a convergence criterion of 1×10-4 residual of the root-mean-squares.

The results of the CFD simulation were validated by comparing the resulting pressure coefficients at different surfaces. Figure 4 and 5 compares the mean pressure coefficients from the wind tunnel test and the CFD simulation at the eaves, and roofs and walls, respectively.

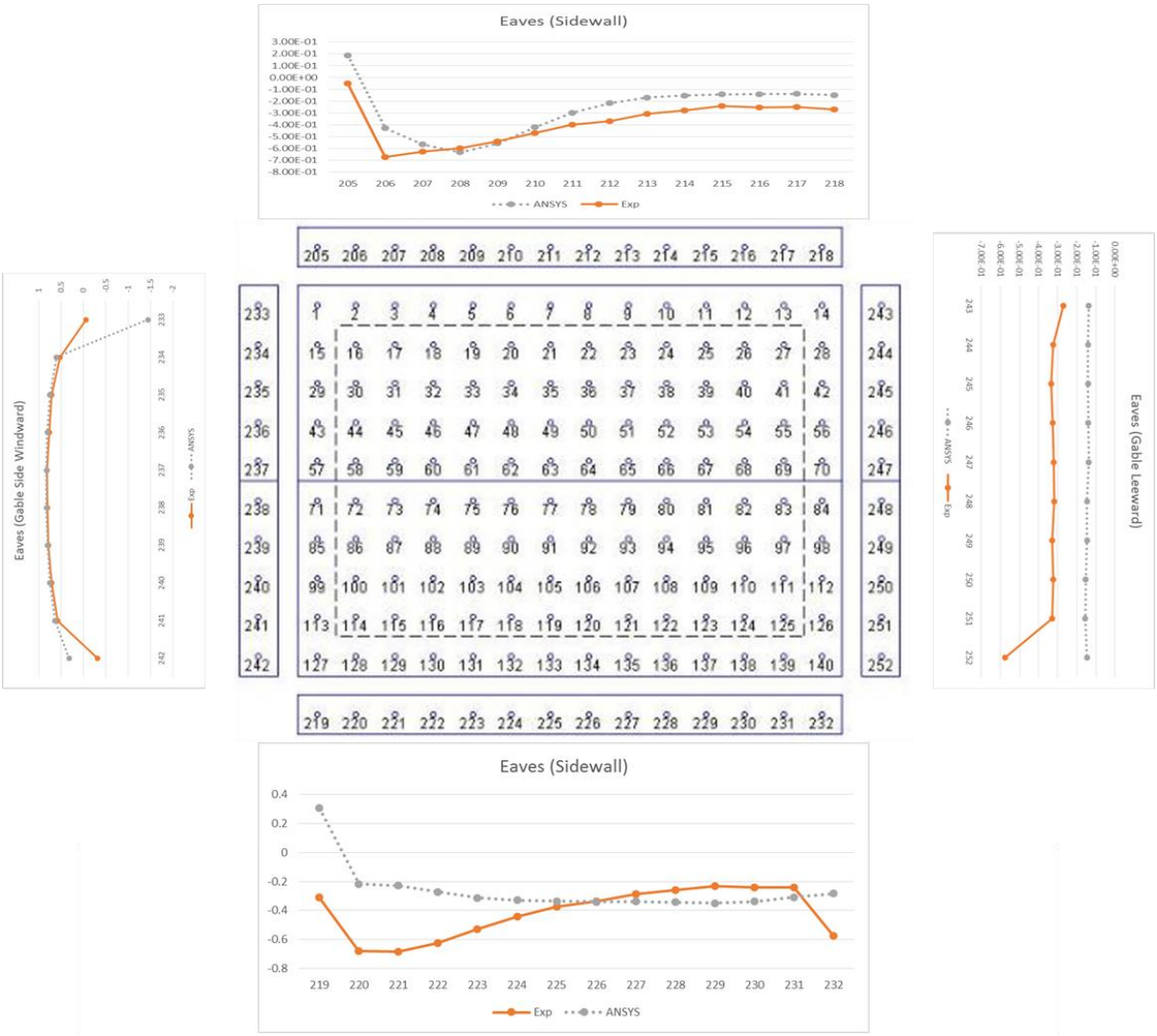

Figure 4. Superimposed mean pressure coefficients at the eaves from the numerical simulation and wind tunnel test results of a TPU model of isolated low-rise building with eaves of roof type C and having an aspect ratio of 1:4.

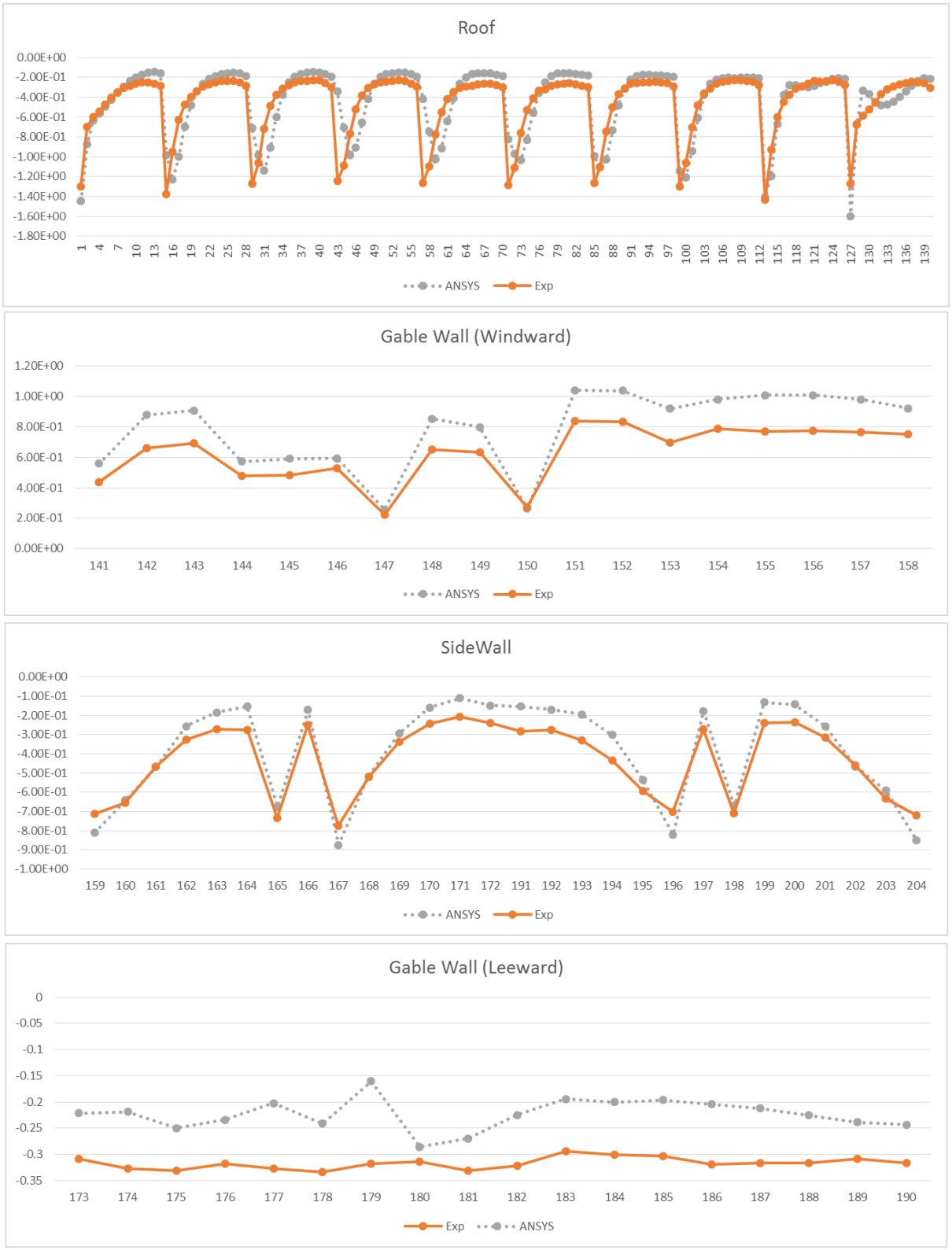

Figure 5. Superimposed mean pressure coefficients at the roof and wall surfaces from the numerical simulation and wind tunnel test results of a TPU model of isolated low-rise building with eaves of roof type C and having an aspect ratio of 1:4.

2.4 Failure Assessment

The flowchart used in the failure assessment is shown in Figure 6. Using the information on the building configuration and dimensions, the critical building components were discretised into building elements. Moreover, the failure simulation also considers the damage propagation in the roof system as illustrated in Figure 7. Since failure in the roof components is assessed at uplift, the direction of the damage propagation was set to proliferate upwards. This means that when a particular roof element fails, all the overlying roof components within its tributary area will be deemed damaged. To illustrate the damage propagation, if a truss element fails, then all the purlin sections overlying that truss will also fail, resulting in their removal. Consequently, the roof panels overlying the removed purlins together with the roof fasteners connected to it will also be removed. For this reason, there is a need to create linkages between the two adjacent roof components – the truss and the purlin, the purlin and the roof panel, and the roof panel and the roof fastener. In other words, the linkages group together the elements of the underlying component to the affected elements above it.

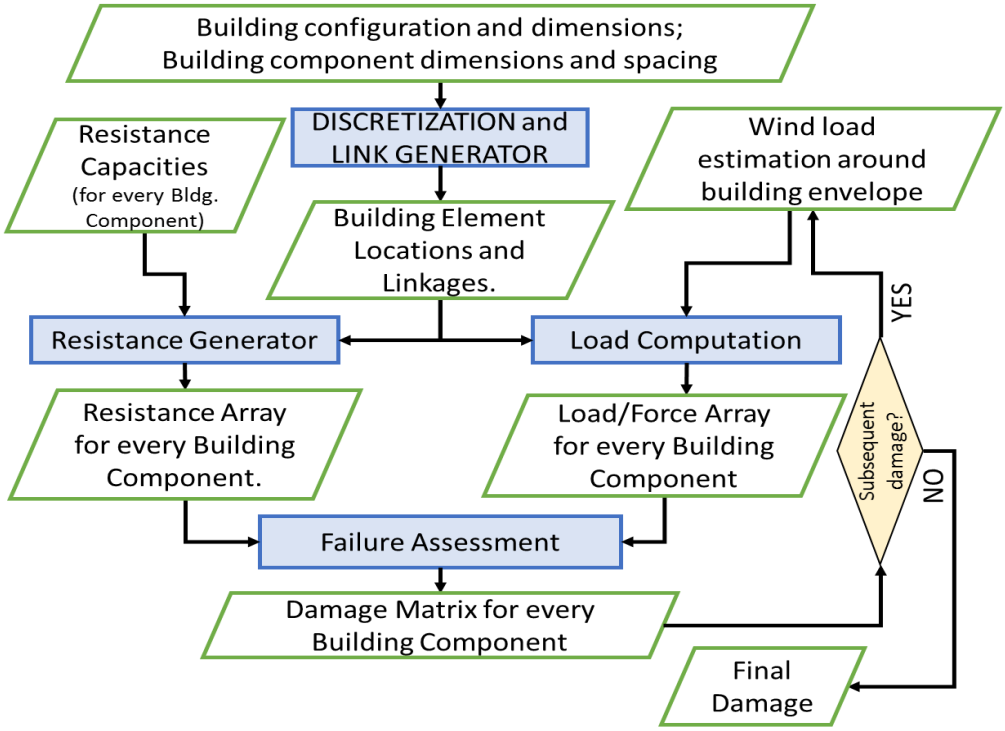

Figure 6. Flowchart of the failure assessment.

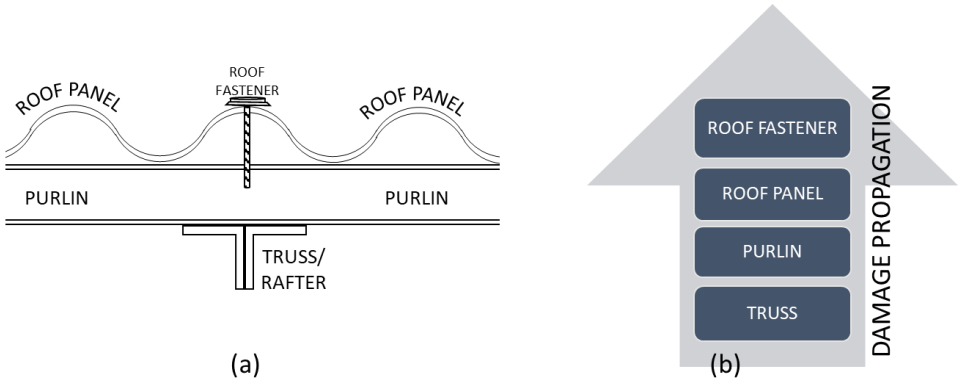

Figure 7. Failure propagation. (a) schematic diagram of the failure propagation at the roof; (b) path of the failure propagation.

After discretising the building into building elements and implementing the appropriate grouping for damage propagation, resistance capacities are randomly generated in each building element using the probabilistic parameters associated with each identified failure mode. A building element can have multiple resistances associated with its identified failure mode/s. This is true for the roof fasteners having nail pull-out and pull-thru as their failure modes.

Then using the CFD results, the simulated wind pressures were used to estimate the loading at the building element. For the window panels, the wind pressures were directly estimated from the mean pressure coefficients, Cp, derived from the CFD simulation. A structural analysis, however, is used to transmit the wind pressure onto the roof structure elements. The roof system is modelled as frame elements and is loaded with the equivalent concentrated force at the locations of the roof fasteners. The concentrated forces represent the equivalent forces of the pressure on the roof panel, F_{wind}, and the weight coming from the roof cover and the roof fastener, F_{Weight}. The weight is further resolved into x' and y' component using the roof slope , θ. The free-body diagram of the equivalent concentrated force at the locations of the roof fasteners is shown in Figure 8 and is computed using the following equations.

$$\vec{F}_{screw} = -F_{Weight} \sin\theta \ \hat{\boldsymbol{\imath}}' + \left(F_{wind} + F_{Weight} \cos\theta\right) \hat{\boldsymbol{\jmath}}'$$

The equivalent force from the mean pressure coefficients computed from the CFD simulation is estimated as follows.

$$F_{wind} = \frac{\rho_{air} v_{ref}^2}{2} C_{pnet} A_{trib}$$

ρ_{air} is the air density, v_{ref} is the reference velocity, C_{pnet} is the net mean pressure coefficient, and A_{trib} is the tributary area at the associated roof fastener.

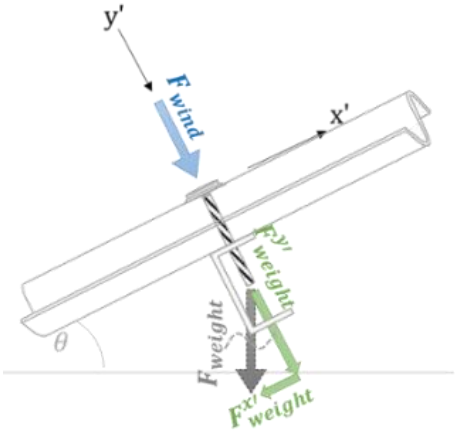

Figure 8. Free-body diagram in estimating the equivalent force at the roof fastener considering wind pressure and roof weight.

After the resistance values and the corresponding forces are quantified at the building elements, the evaluation of the failure will then follow. Failure is defined when the resistance capacity is exceeded by the estimated load.

The result of the failure assessment is damage probabilities at the building component level.

2.5 Direct and Propagated Damage

At this point, the failure simulation program can account for the total damage to each building component. However, this cannot determine which building components make the entire building vulnerable, because the total damage of a certain building component can also be attributed to the failure of the underlying components rather than on strength alone. Hence, this study deconstructed the total damage at a particular building component to direct damage or propagated damage.

Direct damage is the failure brought about by the building component's inadequacy in strength. Propagated damage is the damage incurred by the building component due to the failure of an underlying building component.

The damages in the roof were lumped into three major building components – the roof cover, purlin, and the truss. The failure propagation sequence starts from the roof-to-column connections going to the purlin connections and purlin sections, and lastly, the roof cover.

The total damage to the roof cover includes the total damage to the roof panels and roof fasteners. The total damage on the roof panels accounts for the propagated damage from the roof fasteners and the purlin section while the total damage to the roof fasteners accounts for the direct damage at the roof fasteners and the propagated damage from the roof panels. From the described relationship, it is apparent that the total damage at the roof fastener and the roof panels are interdependent. Hence the study employs a two-pass failure evaluation at the roof

fastener. The first pass accounts for the direct damage at the roof fasteners due to the exceedance of the uplift force to the fastener's resistance denoted as RF_DDi. And the second pass accounts for the removal of fasteners contained in a damaged roof panel, RF_DDf. The entire roof panel containing at least one failed fastener is deemed failed and is regarded as the direct damage to the roof panel, Pa_DD. The direct damage to the roof panel was combined with the propagated damage from the failure of the purlin sections (Pa_PD_PSSum) to come up with the total damage of the roof panels (Pa_Sum).

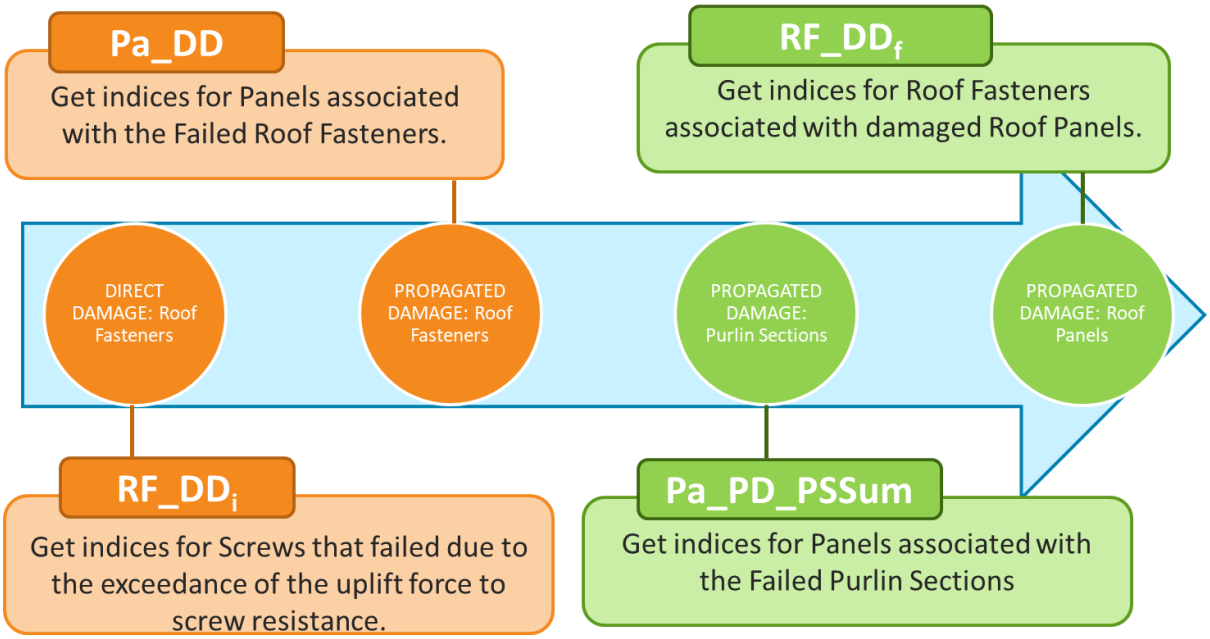

Figure 9. Failure sequence for the roof cover.

The total damage at the purlin component is comprised of the total damage of the purlin connection (PC_Sum) and the total damage of the purlin section (PS_Sum). The total damage at the purlin connection is the sum of the damage counts due to direct damage (PC_DD) and the propagated damage from the failure of the roof-to-column connection (PC_PD_RCC). The direct damage of the purlin connection is defined as the exceedance of the resultant force at the purlin connection to the computed weld connection resistance. On the other hand, the total damage at the purlin section (PS) is attributed to direct damages and propagated damages from the failure of the roof-to-column connection and the purlin connection. The direct damage of the purlin section (PS_DD) resulted from the exceedance of the stress developed in the section to its section capacity. The propagated damage from the roof-to-column connection (PS_PD_RCC) comes from the failure of the truss that propagates to the overlying components within its tributary area. And lastly, the propagated damage from the purlin connection (PS_PD_PC) wherein failure of which results to the removal of the connection. Although its failure does not directly translate to the damage of the connecting purlin section, its removal increases the purlin slenderness. Hence the failure of the purlin is determined after the reanalysis of the entire roof framing system.

The following figure illustrates the expected outputs in deconstructing the total damages per component.

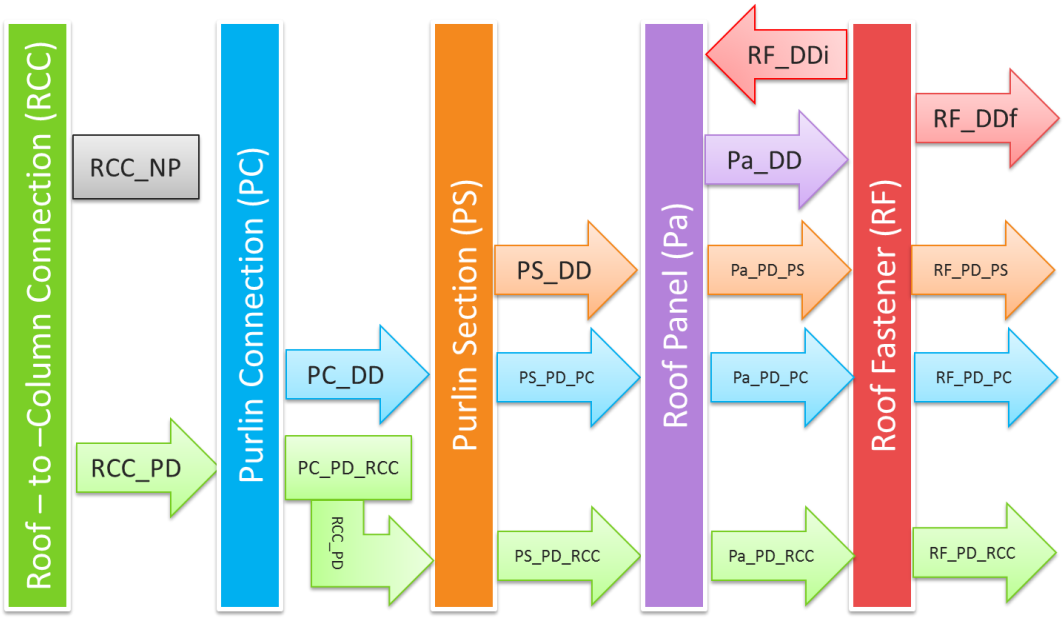

Figure 10. Deconstruction of the total damages per component.

The total number of damaged building elements resulting from the failure assessment at the roof-to-column connection is reclassified into a group of non-propagating (RCC_NP) damage and propagating damage (RCC_PD). RCC_NP does not affect the failure of the overlying components, while RCC_PD passed on to the immediate overlying component – the purlin connection.

There is a possibility that at a particular building component multiple failure events occur. In such cases, the problem to which component should the damage be attributed arises. To address this issue, the author opted to present also a separate count that marks the simultaneous occurrence of failure. Take for example the case of the total damage to purlin section. Although there are only three types of damage at the purlin section, the study further classified this considering the simultaneous failure as a separate count. Hence, the total damage on the purlin section is classified into 7 bins and are illustrated in a Venn diagram in the following figure. This includes the direct damage of the purlin section, propagated damage from the roof-to-column connection, the propagated damage from the purlin connection, simultaneous failure of the purlin section and the roof-to-column connection, simultaneous failure of the purlin connection and the roof-to-column connection, and simultaneous failure of the purlin section, purlin connection and roof-to-column connection.

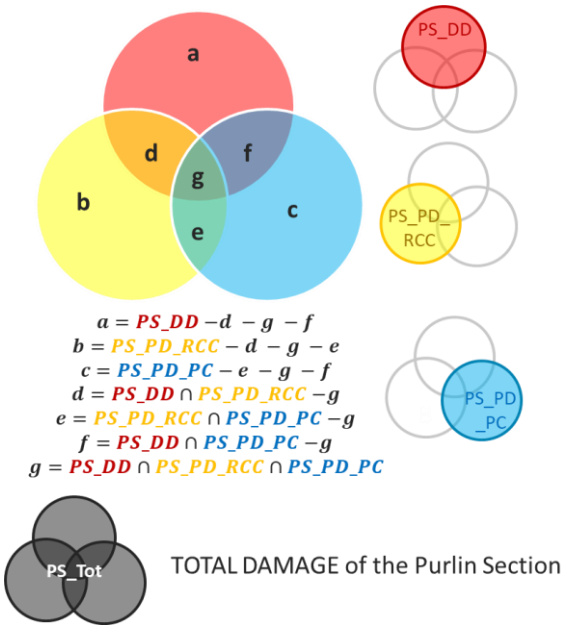

Figure 11. Purlin section total damage decomposition.

The total damage count at the purlin section is passed on to the roof panel failure assessment as a cumulative value (PS_Sum). The propagated damage to roof panel due to purlin (Panel_PD_PS) is broken down back to its seven components by multiplying the propagated damage count, Panel_PD_PS, with the damage percentage of the affecting building component to the total damage of the purlin section. Meaning, the roof panel damage attributed to, say, the direct damage of the purlin section is equal to the ratio of the direct damage of the purlin section, PS_DD, to the total damage of the purlin section, PS_Sum, multiplied to the propagated damage of the roof panel due to the failure of the purlin section (Pa_PSSum).

2.5 Damage Cost Attribution

In order to aggregate the damages from various building components into one representative measure of building damage, the damage counts classified and stored in the previous section is converted to damage costs. The component damage costs were estimated by taking the product of the component damage counts (CDni) and their respective component unit cost (CUCi). The average component damage cost, taken as the ratio of the total component damage cost (CDCi) to the total number of building elements in a building component (i) for all building cases, was then divided by the total cost of construction to estimate the component cost damage ratio (CCDRi). This is exemplified in the following equation.

$$CCDR_i = \frac{\sum_{k=1}^{N} \frac{[\sum_{n=1}^{nd}(CDn_i * CUC_i)_n]_k}{Cn * N}}{Total\ Cost\ of\ Construction}$$

where, n refers to the indices of the damaged building element of a certain building component i, and for a particular building case k. nd refers to the total number of damaged building element. Cn refers to the total number of building elements there are in a building component.

N refers to the total number of building cases considered, and m is the total number of building components considered in the failure simulation. The component damage ratio was estimated by taking the average of the product of the component damage counts (CDni) and their respective component unit cost (CUCi).

The estimation of the component unit costs was determined from the cost of construction and repair of the various building components. This was exemplified in the study of Sapo (Sapo, 2016)[13] and Tan (Tan, 2017)[14].

The damage costs were further categorized and aggregated into sources of damage and are referred to as damage cost attribution. Table 2 maps out the bins created to store the damage counts, while Table 3 shows the variables used to denote the converted damage counts to component cost damage ratios, and Table 4 shows the aggregation of the damage ratios into fifteen (15) damage cost attributions.

Table 2. Established damage count classifications and the corresponding notations used.

	Direct and Propagated Damage					Simultaneous Damage					
Damage to	RCC	PC	PS	Pa	RF	PC ∩ RCC	PS ∩ RCC	PS ∩ PC	PS ∩ PC ∩ RCC	Pa ∩ PS	RF ∩ PS
RCC	RCC_DD										
PC	PC_PD_RCC	PC_DD				PC_PC ∩ RCC					
PS	PS_PD_RCC	PS_PD_PC	PS_DD			PS_PC ∩ RCC	PS_PS ∩ RCC	PS_PS ∩ PC	PS_PS ∩ PC ∩ RCC		
Pa			Pa_PD_PSSum	Pa_DD						Pa_Pa ∩ PSSum	
RF			RF_PD_PSSum	RF_DDf	RF_DDi						RF_RF ∩ PS

Table 3. Conversion of damage counts to cost attributions and the corresponding notations used.

	Direct and Propagated Damage					Simultaneous Damage					
Damage to	RCC	PC	PS	Pa	RF	PC ∩ RCC	PS ∩ RCC	PS ∩ PC	PS ∩ PC ∩ RCC	Pa ∩ PS	RF ∩ PS
RCC	CA2RCC										
PC	CA2RCC	CA2PC				CA2PC_RCC					
PS	CA2RCC	CA2PC	CA2PS			CA2PC_RCC	CA2PS_RCC	CA2PS_PC	CA2PS_PC_RCC		
Pa			CA2PSSum*	CA2RC						CA2RC_PSSum*	
RF			CA2PSSum*	CA2RC	CA2RC						CA2RC_PSSum*

Table 4. Aggregation of cost attributions to building components.

	Direct and Propagated Damage					Simultaneous Damage					
Damage to	RCC	PC	PS	Pa	RF	PC ∩ RCC	PS ∩ RCC	PS ∩ PC	PS ∩ PC ∩ RCC	Pa ∩ PS	RF ∩ PS
RCC	CA2RCC										
PC	CA2RCC	CA2PC				CA2PC_RCC					
PS	CA2RCC	CA2PC	CA2PS			CA2PC_RCC	CA2PS_RCC	CA2PS_PC	CA2PS_PC_RCC		
Pa	CA2RCC	CA2PC	CA2PS	CA2RC		CA2PC_RCC	CA2PS_RCC	CA2PS_PC	CA2PS_PC_RCC	CA2RC_RCC CA2RC_PC CA2RC_PS CA2RC_PC_RCC CA2RC_PS_RCC CA2RC_PS_PC CA2RC_PS_PC_RCC	
RF	CA2RCC	CA2PC	CA2PS	CA2RC	CA2RC	CA2PC_RCC	CA2PS_RCC	CA2PS_PC	CA2PS_PC_RCC		CA2RC_RCC CA2RC_PC CA2RC_PS CA2RC_PC_RCC CA2RC_PS_RCC CA2RC_PS_PC CA2RC_PS_PC_RCC

Plotting the damage cost attribution against increasing wind speed yields a 3D-plot referred to as the damage attribution chart. This chart aids in identifying the building component/s that

results to the highest amount of damage indicated by the peak in the damage ratio.

III. RESULTS AND DISCUSSION

The resulting damage attribution chart for the base design case is shown in Figure 12. It can be concluded that the dominant source of damage was due to the direct damage incurred at the roof-to-column connection (CA2RCC: Damage Cost Attributed to Roof-to-Column Connection). Hence this is the identified critical building component.

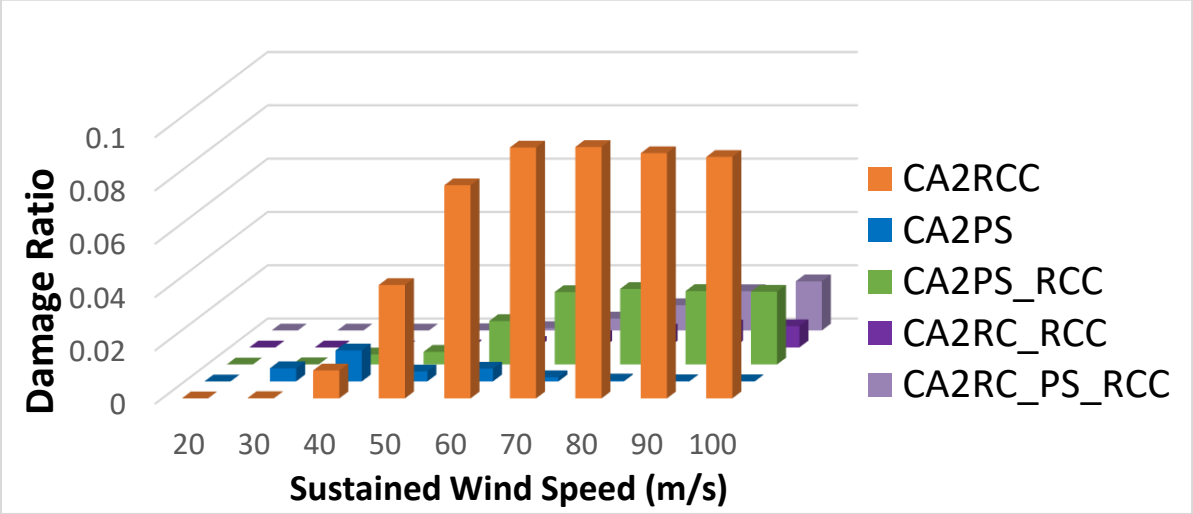

Figure 12. Damage attribution chart for the base design.[CA2RCC – Cost damage Attributed to the failure of the Roof-to-Column Connection (RCC); CA2PS_RCC – Cost damage Attributed to both failure of the Purlin Section (PS) and RCC; CA2RF_PS – Cost damage Attributed to the failure of Roof Faster (RF) and PS; CA2RF_RCC – Cost damage Attributed to the failure of the RF and RCC; CA2RF_PS_RCC – Cost damage Attributed to the failure of the RF, PS, and RCC.]

Further, looking at the 40 -50 m/s (144-180 kph) wind speed, there are 3 outstanding damages. These are the attributed to the failure to RCC, purlin sections, and the simultaneous failure of the purlin sections and RCC.

In the conducted post-disaster survey from typhoon Odette (Dec. 2021), a school building in Mandaue with a similar configuration and roof-to-column connection was surveyed. The estimated maximum gust wind speed in the area based on the Philippine Atmospheric, Geophysical, and Astronomical Services Administration (PAGASA) at Mactan station is 167 kph. Figure 13 shows the before and after photos of the school building that illustrates the extent of damage of the Typhoon Odette.

(a)

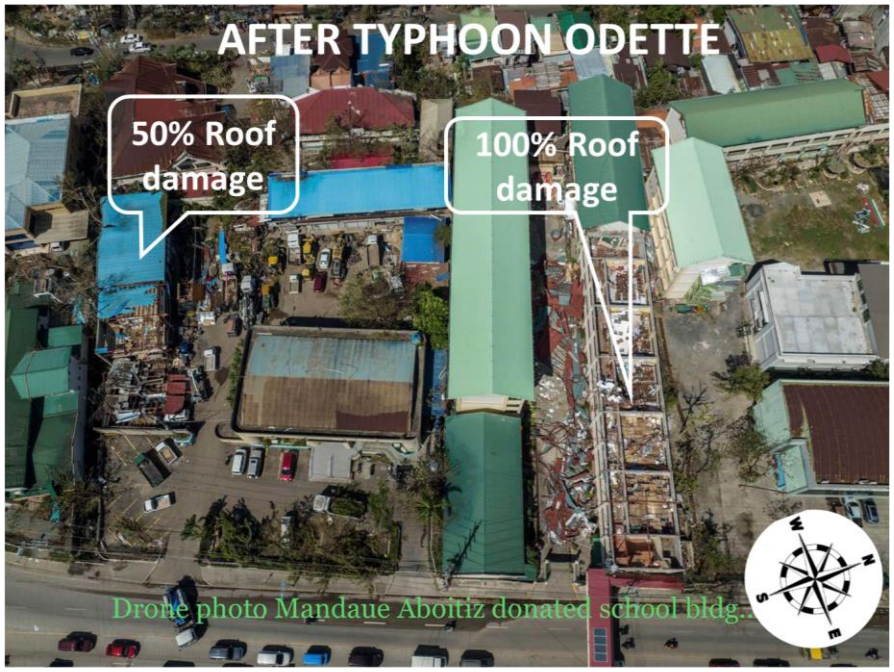

(b)

Figure 13. (a) Satellite image taken from Google Earth[7] before Typhoon Odette. (b) Drone shot of the aerial view of the school building after the Typhoon Odette. Courtesy of Engr. Peter Paul Dy (taken Dec. 2021)[6]

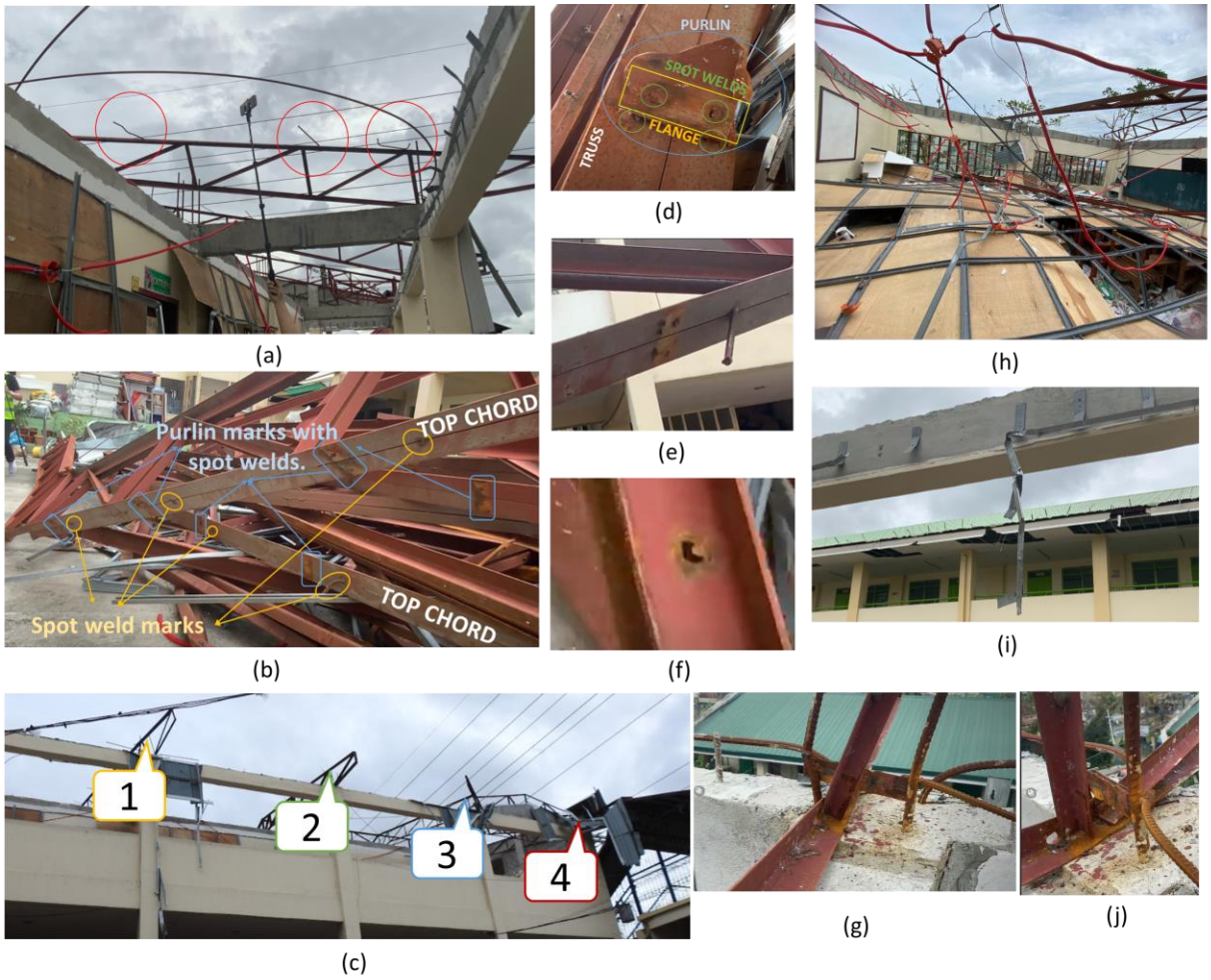

Figure 14. Observed failures in the school building due to Typhoon Odette. (a): Failure of the rebar used as purlin connections to the truss; (b): Observed connection marks on the blown-off roof trusses; (c): Remaining connected trusses; (d): Spot welds on the flange and edge of the purlin; (e): Protruding rebar used as purlin connection; (f): Burned markings around the hole on the purlin web; (g) shows a section view of the roof-to-column connection across the plane of the truss; (h): Observed ceiling collapse due to framing failure.; (i) ceiling frame connection failure; (j) shows a profile view of the RCC parallel to the truss .(by Tan, 2021)[15]

Figure 14.c shows the four remaining trusses out of 11. Note that the roof trusses found on the ground were all intact, as observed in Figure 14.b., suggesting that connection failure was the root cause of the damage. Figure 14.g and 14.j show the details of the roof truss connection. Purlin failure observed was also mostly due to the connection failure as can be observed from Figures 14.a, 14.d, and 14.e. Figure 14.f. shows evidence of tearing at the purlin section near the welded area. All these observed failures were consistent with the results of the simulation. Figures 14.h and 14.i shows failure of the ceiling, which was not monitored in the failure simulation in this study since it is non-structural. But the extent of damage is significant that the study recommends it be considered in the framework.

Lastly, at the extreme wind speed range, 70-100 m/s (252 – 360 kph), the dominant source of failure is still the roof-to-column connection and then followed by the simultaneous failures of the roof covers, purlin sections, and roof-to-column connection.

It is also interesting to see how will the amount of damage be affected by strengthening specific building components. This study further explored three design cases – strengthened RCC using anchor bolts, strengthened roof fasteners using J-bolts, and increased purlin section. The resulting vulnerability curves are shown in Figure 15.

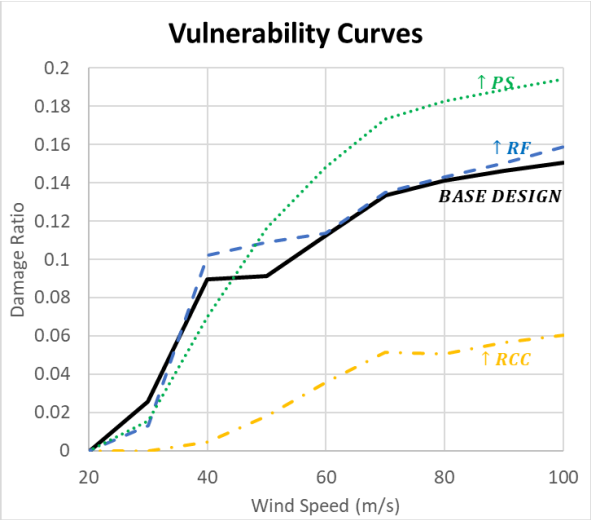

Figure 15. Vulnerability curves of the base design (black solid line); design case of increased roof-to-column connection (RCC) capacity (yellow dot-dash line); design case of increased roof fastener (RF) capacity (blue dashed line); design case of increased purlin section (PS) capacity (green dotted line).

The large reduction in the amount of damage is apparent when RCC was strengthened following the result of the damage attribution chart. Strengthening the roof fastener barely affects the amount of damage, since the damages incurred are not mainly attributed to roof fasteners as referred to the damage attribution chart. Strengthening the purlin section, however, would result in a larger building damage. From the damage attribution chart in Figure 12, purlin sections are next to roof-to-column connections where source of damage can be traced. Strengthening the purlins, results to the load transfer to the roof-to-column connection, which then results to more damaged roof-to-column connection that also affected the overlying components. Hence resulting to a larger building damage.

IV. CONCLUSION

This study employs a fault tree analysis incorporated into the failure simulation program that classified the damage at the building component level. For each building component, the damage was classified into either direct damage or propagated damage. Consequently, the

propagated damage was further classified based on the source of damage. Thus, damages incurred by the overlying components can be attributed to the failure of the underlying components.

With the addition of the fault tree analysis into the failure simulation, the study was able to develop what it coined as the damage attribution chart. This chart enables the determination of the critical building component where strengthening methods may be focused. The proposed framework was applied to a standard school building where the resulting critical building component was found to be the roof-to-column connection followed by the failure of the purlin sections. This was validated against a post-damage survey on a similar structure that was damaged by the Typhoon Odette. The study further investigates what happens when various building components were strengthened. Three strengthening schemes were investigated – use of a roof fastener with higher pull-out capacity, increasing the purlin section, and the use of an anchor bolt at the roof-to-column connection. The resulting vulnerability curves suggests that strengthening the critical component can drastically reduce the amount of overall building damage. In this case, strengthening of the roof-to-column connection identified as the critical component based from the damage attribution chart shall reduce the damage ratio by around 10%. While strengthening other components may either result to an insignificant reduction, as in the case of strengthening the roof fastener, or even worsen the overall building damage, as in the case of increasing the purlin section. These results further support the findings in Nishijima's[10] study which concluded that not all strengthening mitigations would lead to lesser damage.

The damage attribution chart developed in this study can determine the critical building component and provide a structured process in the design optimization process against the severe wind.

V. RECOMMENDATIONS

The proposed method is highly dependent on how the load path and failure mechanisms were defined. Although it yields reasonable results as assessed by relative comparison to the resulting vulnerability curves and comparison with observed damage of a similar structure, further and more extensive and quantifiable validation is recommended to substantiate and build more confidence in the results. It is recommended to collect or conduct post-damage surveys of similar structures. Conduct of a system test as a form of validation of the failure model is also recommended.

Based on the post-damage survey presented, it is also recommended to consider the ceiling system as part of the vulnerable component, albeit non-structural. Development of the internal pressure transmitted onto the ceiling and to the truss could have contributed to the failure of the RCC.

The creation of a database of resistance capacities of various building components is recommended for design optimization purposes.

VI. ACKNOWLEDGEMENTS

This research was funded by the Thesis and Dissertation Grant provided by the Office of the Chancellor of the University of the Philippines Diliman, through the Office of the Vice Chancellor for Research and Development.

We would like to acknowledge that this collaborative work has been conducted partly under the J-RAPID project funded by Japan Science & Technology (JST) under the working title, "Investigation of wind damage processes by Typhoon Yolanda, identification of effective damage reduction measures, and its facilitation to recovery work".

We thank our colleagues from the Wind Engineering and Wind Resistant Structures Laboratory of the Disaster Prevention Research Institute (DPRI) of Kyoto University headed then by Dr. Takashi Maruyama, together with Dr. Kazuyoshi Nishijima and Dr. Hiroaki Nishimura who provided their insights and expertise that greatly assisted the research.

We would also like to express our gratitude to the research group headed by Dr. Yukio Tamura together with Dr. Masahiro Matsui and Dr. Kim Wonsul of Tokyo Polytechnic University, for promptly providing advice regarding the wind tunnel testing.

References:

[1] American Society for Testing Materials Standard E1300-12a. 2012. Standard practice for determining load resistance of glass in buildings. West Conshohocken, PA: ASTM International.

[2] ANSYS® n.d., Academic research for computational fluid dynamics. Release 15.0. computer software. ANSYS Inc. Canonsburg, PA USA.

[3] Bisa H. 2013. Empirical threshold values of roof connections using pull-out test on nails and screws. [undergraduate]. Institute of Civil Engineering: University of the Philippines – Diliman.

[4] Cope, A. 2004. Predicting the vulnerability of typical residential buildings to hurricane damage. [doctoral]. University of Florida.

[5] Doguiles AER. 2015. Failure modeling of roof-truss supports of reinforced concrete frame residential buildings due to severe wind. [undergraduate]. Institute of Civil Engineering: University of the Philippines – Diliman.

[6] Dy PP. 2021, Dec. aerial photo of school building in Mandaue that was damaged by the Typhoon Odette. Philippine Institute of Civil Engineering (PICE).

[7] Google Earth. n.d., [Google Earth satellite image of Mandaue City Comprehensive National High School]. Retrieved Dec. 21, 2021.

[8] Goyal P, Datta T and Vijay V. 2012. Vulnerability of rural houses to cyclonic wind. International Journal of Disaster Resilience in the Built Environment. 3(1):20-41.

[9] AISC. 2008. Retrieved from https://www.aisc.org/globalassets/aisc/research-library/strength-and-ductility-of-welded-joints-subjected-to-out-of-plane-bending.pdf.

[10] East Asia Science and Innovation Area Joint Research Program. 2015. Retrieved from https://www.the-easia.org/jrp/pdf/w05/Nishijima-Espina.pdf.

[11] Pinelli J, Gurley K, Subramanian C, Hamid S, Pita G. 2008. Validation of a probabilistic model for hurricane insurance loss projections in Florida. Reliability Engineering & System Safety. 93(12):1896-1905.

[12] Sanidad J. 2016. Determination of resistance capacities against thread failure and unbending of J-bolts used as roof fasteners. [undergraduate]. Institute of Civil Engineering: University of the Philippines –

Diliman,
[13] Sapo E. 2016. Wind vulnerability assessment of DepEd standard one-storey one classroom in Albay using fault tree analysis. [undergraduate] Institute of Civil Engineering: University of the Philippines – Diliman.
[14] Tan LRE. 2017. Wind vulnerability assessment of enhanced wind resilient design for a standard one-story school building in Tacloban using component-based approach in reliability modeling. [masteral]. Institute of Civil Engineering: University of the Philippines – Diliman.
[15] Tan LRE. 2021. Damage photos of Mandaue City Comprehensive National High School due to Typhoon Odette. University of the Philippines - Institute of Civil Engineering.
[16] Torkian BB, Pinelli JP, Gurley KR, Hamid S. 2014. Cost-and-benefit evaluation of windstorm damage mitigation techniques in Florida. Natural Hazards Review. 15(2): 150-157.
[17] Tokyo Polytechnic University. Retrieved from www.wind.arch.t-kougei.ac.jp/info_center/windpressure/lowriseeave/Introductionofthedatabase.pdf.
[18] Unanwa C, McDonald J, Mehta K, Smith D. 2000. The development of wind damage bands for buildings. Journal of Wind Engineering and Industrial Aerodynamics. 84(1):119-149.
[19] UPD-ICE. 2013. Development of vulnerability curves of key building types in the Greater Metro Manila Area, Philippines. Quezon City: University of the Philippines.
[20] Zhang S, Nishijima K, Maruyama T. 2014. Reliability-based modeling of typhoon induced wind vulnerability for residential buildings in Japan. Journal of Wind Engineering and Industrial Aerodynamics. 124:68-81.